

Origin of the asymmetry in martensitic phase transitions in off-stoichiometric NiTi near equiatomic compositions

Zhigang Wu^{1,*}, John W. Lawson^{1,†} and Othmane Benafan²

¹*Intelligent Systems Division, NASA Ames Research Center, Moffett Field, California 94035, USA*

²*Materials and Structures Division, NASA Glenn Research Center, Cleveland, Ohio 44135, USA*



(Received 14 July 2023; accepted 27 September 2023; published 12 October 2023)

Nitinol (NiTi) is the most commonly used and most extensively studied shape memory alloy (SMA). However, it remains a mystery that a small increase of Ni concentration (x_{Ni}) from 50% to 51% in NiTi results in a dramatic drop of about 110 K in the martensitic transition temperature (MTT), while a similar increase of Ti barely changes MTT. This weird behavior drastically affects both the manufacturing and applications of the NiTi-based SMAs, which represent the majority of ongoing scientific research efforts in this field. Using the most accurate first-principles methods, we find that this trend in MTT can be well reproduced theoretically. Furthermore, the physical origin of this striking asymmetry in MTT is revealed to be the fact that the atomic size of Ni is much larger than that of Ti in NiTi; though for free atoms, Ti is larger than Ni. Replacing smaller Ti atoms with bigger Ni atoms in NiTi leads to a much larger deviation from the ideal cubic B2 structure in the austenite phase than does the other way around.

DOI: [10.1103/PhysRevB.108.L140103](https://doi.org/10.1103/PhysRevB.108.L140103)

Introduction. Shape memory alloys (SMAs) can recover their original shapes upon heating [1–3] due to the existence of a reversible martensitic transition between the high-temperature austenite and low-temperature martensite phases. SMAs have a wide range of potential applications in aerospace, civil engineering, bioengineering, etc. [1–7]. In order to create new SMAs that are operable at a target temperature range, the most common approach is alloying a binary with other metals to form ternaries, quaternaries, pentanaries, etc.; among them, the NiTi-based multicomponent SMAs have attracted tremendous research efforts lately [7–15].

However, the concentration of Ni (x_{Ni}) in these multicomponent SMAs could drastically affect their thermodynamics and properties [7–15]. This stems from a well-known, but poorly understood fact that slightly increasing x_{Ni} (e.g., from 50% to 51%) in NiTi will dramatically decrease its martensitic transition temperature (MTT) (by ~ 110 K), while increasing the Ti concentration (x_{Ti}) by the same amount barely changes the MTT [16–19]. Even though NiTi is arguably the most important, most studied, and most commonly used SMA [20–32], this unusual behavior has hardly been investigated theoretically, especially from first principles, after it was discovered over 60 years ago.

The dependence of the thermodynamics of NiTi on Ni concentration is not only of substantial scientific interest, but also of paramount technological consequence. For example, the equiatomic NiTi is used in thermal and electric actuators such as fluidic thermal valves, pneumatic valves, and optical image stabilizer in mobile phones. On the other

hand, the Ni-rich NiTi is used in biomedical applications, including medical stents, due to precipitation strengthening. As mentioned above, the properties and applications of the NiTi-based multicomponent SMAs also sensitively depend on the Ni concentration.

In this Letter, we study this dependence using highly accurate *ab initio* molecular dynamics (AIMD) simulations and thermodynamic integration to evaluate the Gibbs free energy (G) for the austenite and the martensite phases as functions of temperature (T) vs x_{Ni} . Not only do our results reproduce the trend of MTT in off-stoichiometric NiTi, but our theoretical analyses also elucidate the origin of this striking asymmetry in MTT vs Ni/Ti concentration, which is largely due to the charge distribution in the NiTi crystal, causing Ni atoms to have a much larger effective size than Ti atoms.

Methodologies. We follow the expression and procedure as described in Ref. [32] to compute the Gibbs free energy,

$$G(T) = E_{\text{ref}}[V(T)] + F^{\text{el}}(T) + F_{\text{h}}^{\text{ph}}(T) + F_{\text{anh}}^{\text{ph}}(T). \quad (1)$$

Here, E_{ref} is the total electronic energy for the reference structure, whose volume (V) is optimized at T . $F^{\text{el}}(T)$ is the electronic free energy given by

$$F^{\text{el}}(T) = U^{\text{el}}(T) - TS^{\text{el}}(T). \quad (2)$$

We followed Ref. [33] to compute the electronic internal energy $U^{\text{el}}(T)$ and the electronic configurational entropy $S^{\text{el}}(T)$, using the self-consistent approach and 20 uncorrelated MD snapshots at each considered temperature.

$F_{\text{h}}^{\text{ph}}(T)$ is the harmonic part of the phonon free energy, and the anharmonic part of the phonon free energy, $F_{\text{anh}}^{\text{ph}}(T)$, is obtained using thermodynamic integration,

$$F_{\text{anh}}^{\text{ph}}(T) = \int_0^1 \left\langle \frac{\partial U(\lambda)}{\partial \lambda} \right\rangle_{\lambda} d\lambda. \quad (3)$$

*zhigang.wu@nasa.gov

†john.w.lawson@nasa.gov

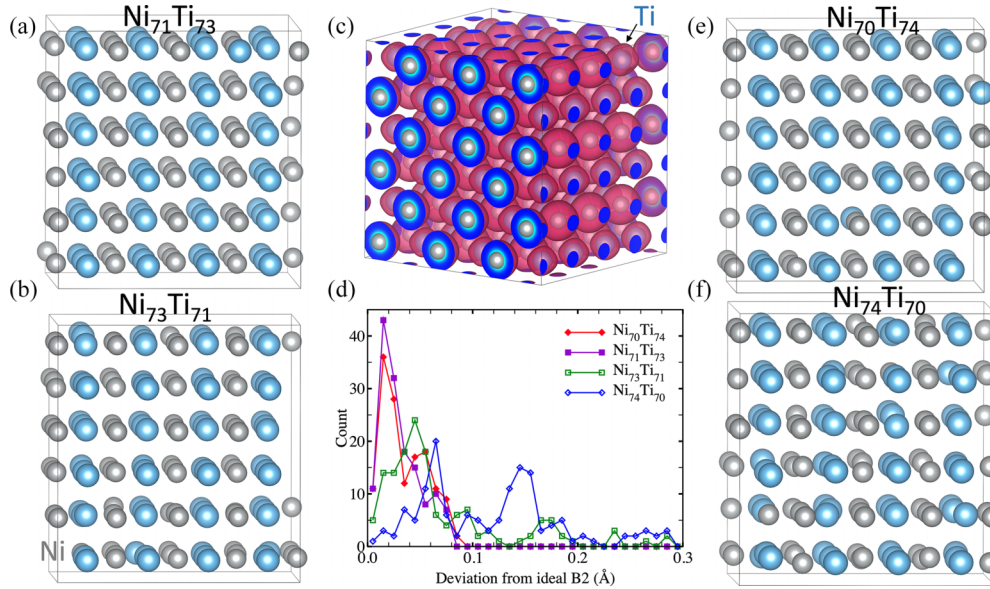


FIG. 1. The obtained reference structures of the austenite phase of (a) $\text{Ni}_{71}\text{Ti}_{73}$, (b) $\text{Ni}_{73}\text{Ti}_{71}$, (e) $\text{Ni}_{70}\text{Ti}_{74}$, and (f) $\text{Ni}_{74}\text{Ti}_{70}$. The Ni atoms and Ti atoms are denoted by gray and sapphire balls, respectively. (c) The electronic density isosurface at 0.041 (electrons/ \AA^3) for $\text{Ni}_{71}\text{Ti}_{73}$, while the minimum and maximum values of electronic density are 0.0214 and 2.057, respectively. (d) The histograms of atomic displacements (deviation) from the ideal B2 structure for $\text{Ni}_{70}\text{Ti}_{74}$, $\text{Ni}_{71}\text{Ti}_{73}$, $\text{Ni}_{73}\text{Ti}_{71}$, and $\text{Ni}_{74}\text{Ti}_{70}$.

Here, $U(\lambda)$ is a mixing of the harmonic potential and the density functional theory (DFT) potential with a mixing parameter λ .

Total-energy calculations and AIMD simulations were carried out using DFT implemented in the VASP package [34–37], while the thermodynamic average $\langle \frac{\partial U}{\partial \lambda} \rangle$ for a fixed λ is obtained from the NVT AIMD simulations with the mixed potential $U(\lambda)$ for 10 to 20 ps, to ensure the error bar of $F_{\text{anh}}^{\text{ph}}$ is less than 0.1 meV/atom. $\lambda = 0.0, 0.25, 0.50, 0.75, 1.0$ are used for integration in Eq. (3) to ensure convergence; the time step is 2.0 fs and the friction factor for the Langevin thermostat is 100 fs.

We employed the up-sampled thermodynamic integration using Langevin dynamics (UP-TILD [38]) to evaluate $F_{\text{anh}}^{\text{ph}}$. Specifically, AIMD simulations were performed with an energy cutoff (E_{cut}) of 300 eV and ~ 3500 \mathbf{k} points per reciprocal atom (KPPRA, i.e., the multiplication of the number of \mathbf{k} points used in reciprocal space and the number of atoms in a unit cell in real space), while the up-sampling of $\Delta U^{\text{DFT}} = U_{\text{high}}^{\text{DFT}} - U_{\text{low}}^{\text{DFT}}$ was done with $E_{\text{cut}} = 450$ eV and ~ 27000 KPPRA, which were also used for total-energy and lattice dynamics calculations to ensure convergence.

The PBE (parametrized by Perdew, Burke and Ernzerhof [39]) density functional and the projector augmented wave (PAW [40,41]) method were used in the DFT calculations. We note that in order to compute the electronic energy and lattice vibrations and to consistently carry out AIMD simulations, i.e., using the same density functional, the best choice is PBE. The valence of Ni and Ti atoms includes $3d^94s^1$ and $3d^24s^2$ electrons, respectively.

Austenite reference structures. The MTT of equiatomic NiTi, corresponding to the transition between austenite B2 (cubic $Pm\bar{3}m$) and martensite B19' (monoclinic $P2_1/m$, with a monoclinic angle $\gamma \approx 98^\circ$ [42,43]), was calculated to be 422 K using 144-atom supercells [32], in comparison with

the averaged experimental data T_0 of 345 K [44–46]. Here, $T_0 = (M_s + A_f)/2$, with M_s and A_f the martensite start and austenite finish temperature, respectively. We note that the predicted MTT is about 77 K higher than the measured T_0 , which is largely due to the fact that both defects (such as antisites) and residual strain are not included. Both are expected to reduce the transition temperature because the resulting cubic phase will deviate from the ideal B2 structure with the $Pm\bar{3}m$ symmetry.

In contrast to the well-defined ideal B2 structure in equiatomic NiTi, which can be used as the reference in thermodynamic integration, the reference structure of the austenite phase of the off-stoichiometric NiTi does not have the $Pm\bar{3}m$ symmetry. We adopt the method described and employed in Ref. [47], and the austenite reference structure of the off-stoichiometric NiTi is obtained by averaging 25 000 AIMD snapshots (50 ps) at 1000 K, as plotted in Figs. 1(a), 1(b), 1(e), and 1(f) for $\text{Ni}_{71}\text{Ti}_{73}$, $\text{Ni}_{73}\text{Ti}_{71}$, $\text{Ni}_{70}\text{Ti}_{74}$, and $\text{Ni}_{74}\text{Ti}_{70}$, respectively.

Here we note that each Ni (or Ti) atom in the B2 structure of equiatomic $\text{Ni}_{72}\text{Ti}_{72}$ is equivalent, so there is only one inequivalent $\text{Ni}_{71}\text{Ti}_{73}$ (or $\text{Ni}_{73}\text{Ti}_{71}$) obtained by replacing one Ni atom (or Ti atom) with one Ti atom (or Ni atom). Then, $\text{Ni}_{70}\text{Ti}_{74}$ (or $\text{Ni}_{74}\text{Ti}_{70}$) is constructed by replacing one more Ni atom (or Ti atom) with one Ti atom (or Ni atom), which has the largest distance from the previously replaced Ni atom (or Ti atom). The austenite phase of off-stoichiometric NiTi is maintained as cubic, while its martensite phase is monoclinic ($\gamma = 98^\circ$), whose lattice vectors and internal coordinates are relaxed. To be consistent with the notations used in experiment and for equiatomic NiTi, for off-stoichiometric NiTi, we still denote the cubic austenite phase as B2 and the monoclinic martensite phase as B19', though they do not possess the $Pm\bar{3}m$ and $P2_1/m$ symmetries, respectively.

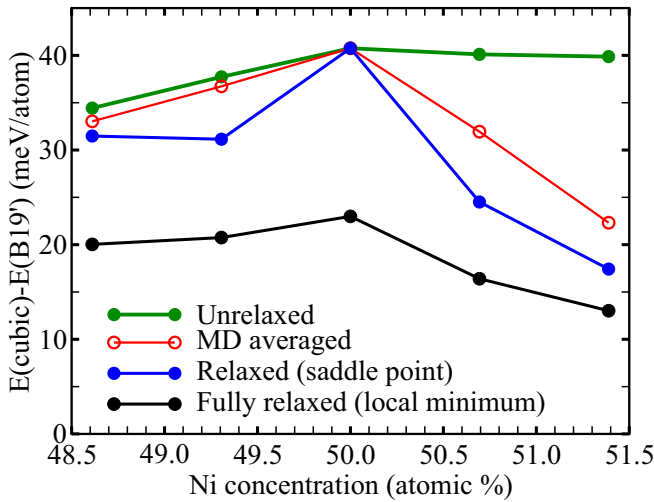


FIG. 2. The energy differences between four different cubic structures and the monoclinic (B19') structure vs Ni concentration. Each unrelaxed structure is relaxed at 0 K and annealed from 1000 to 0 K (fully relaxed). The cubic lattice of each of these four structures is also relaxed at 0 K.

Comparing the reference B2 structures of $\text{Ni}_{71}\text{Ti}_{73}$ and $\text{Ni}_{70}\text{Ti}_{74}$ with those of $\text{Ni}_{73}\text{Ti}_{71}$ and $\text{Ni}_{74}\text{Ti}_{70}$, as plotted in Fig. 1, one finds that the Ni-rich NiTi B2 structures deviate from the ideal B2 ($Pm\bar{3}m$) substantially more than the corresponding Ti-rich NiTi B2 structures, as illustrated by the histograms in Fig. 1(d), where the deviation from the ideal B2 structure is defined as the distance between two corresponding atoms, i.e., one in off-stoichiometric NiTi and the other one in ideal B2 with the same lattice constant.

This is also demonstrated by the energy difference ($\Delta E_{\text{un-MD}}$) between the unrelaxed (green symbols, just replacing atoms in ideal B2) and the MD averaged (red symbols) structures, as plotted in Fig. 2. For the Ti-rich $\text{Ni}_{71}\text{Ti}_{73}$ and $\text{Ni}_{70}\text{Ti}_{74}$, $\Delta E_{\text{un-MD}} = 1.0, 1.4$ meV/atom, respectively, compared with $\Delta E_{\text{un-MD}} = 8.2, 17.6$ meV/atom for Ni-rich $\text{Ni}_{73}\text{Ti}_{71}$ and $\text{Ni}_{74}\text{Ti}_{70}$, respectively. Figure 2 also plots the energies of the relaxed (at 0 K without modifying the symmetry and resulting in a saddle point on the energy surface) and annealed (fully relaxed, without maintaining the original symmetry and resulting in a local minimum) cubic structures for these compositions, setting the monoclinic B19' as zero energy. The same energetic trends are found for the relaxed and fully relaxed structures, though the magnitudes of ΔE between the unrelaxed and the fully relaxed ones become quite similar for these four off-stoichiometric and equiatomic NiTi.

In order to understand in the austenite phase why replacing Ti by Ni leads to a much larger deviation from the ideal B2 than replacing Ni by Ti, we plot the electronic density isosurface of $\text{Ni}_{71}\text{Ti}_{73}$ at 0.041 (electrons/ \AA^3) in Fig. 1(c). The “effective” atomic radius (determined by isosurface) of Ni (1.19 \AA) is about 40% larger than that of Ti (0.83 \AA) in NiTi, while for free atoms, Ni has a smaller size than Ti, e.g., the atomic, valence, and van der Waals radii of Ni are 1.24, 1.24, and 1.63 \AA , respectively, compared with the corresponding values for Ti of 1.47, 1.60, and 2.15 \AA . A larger atom (Ni)

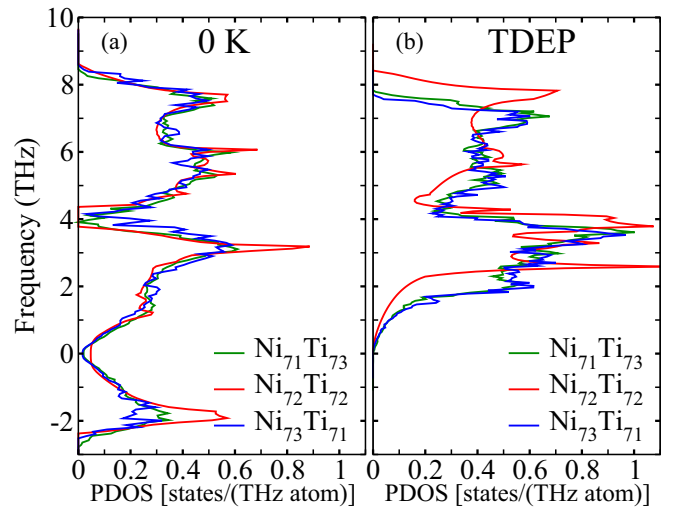


FIG. 3. Phonon density of states (PDOS) for the reference structures of the austenite phase of $\text{Ni}_{71}\text{Ti}_{73}$, $\text{Ni}_{72}\text{Ti}_{72}$, and $\text{Ni}_{73}\text{Ti}_{71}$ at (a) 0 K and (b) high temperature using TDEP. Here, TDEP PDOS for $\text{Ni}_{72}\text{Ti}_{72}$ is obtained at 400 K, while for $\text{Ni}_{71}\text{Ti}_{73}$ and $\text{Ni}_{73}\text{Ti}_{71}$, it is obtained at 1000 K.

replacing a smaller atom (Ti) in NiTi leads to more structural reorganization than a smaller atom replacing a larger one; and this could also be understood by the fact that a Ni atom has 10 valence electrons, while Ti has 4, so replacing Ti by Ni significantly increases the Coulomb repulsion.

Martensitic transition temperature. Similar to equiatomic NiTi, the reference structure of the austenite phase of off-stoichiometric NiTi is unstable at 0 K with negative phonons, and it can be stabilized by entropy at high temperature, employing the temperature-dependent effective potential (TDEP) [48,49] method, as demonstrated by the phonon density of states plotted in Fig. 3 for $\text{Ni}_{71}\text{Ti}_{73}$ and $\text{Ni}_{73}\text{Ti}_{71}$, in comparison with those of $\text{Ni}_{72}\text{Ti}_{72}$. We note that for off-stoichiometric NiTi, higher temperature and longer simulation time are needed to obtain converged TDEP interatomic force constants (IFCs) than for equiatomic NiTi because of lower symmetry and the larger number of independent IFCs.

Next, we computed the Gibbs free energy G for the austenite and martensite phases. In Fig. 4(a), we plotted ΔG vs temperature for these four off-stoichiometric NiTi, in comparison with the equiatomic NiTi. We find that for Ti-rich $\text{Ni}_{71}\text{Ti}_{73}$ and $\text{Ni}_{70}\text{Ti}_{74}$, ΔG vs T are quite close to that of $\text{Ni}_{72}\text{Ti}_{72}$, and so are the calculated MTTs, as illustrated in Fig. 4(a). However, for Ni-rich $\text{Ni}_{73}\text{Ti}_{71}$ and $\text{Ni}_{74}\text{Ti}_{70}$, ΔG are reduced by about 4 and 8 meV/atom compared with that of $\text{Ni}_{72}\text{Ti}_{72}$ at the same T , mainly due to the much reduced energy difference and leading to much decreased MTTs.

The calculated MTT vs x_{Ni} has exactly the same trend as that of the experimental data [19], as shown in Fig. 4(b). We note that experimentally, such a trend in MTT with respect to composition corresponds to a solutionized material with no secondary phase, such as precipitates. Just like the equiatomic NiTi, the calculated MTTs of the off-stoichiometric NiTi are also consistently about 60–70 K higher than the experimental T_0 . Thus we have demonstrated that the vibrational entropy plays a similarly crucial role in martensitic transitions in

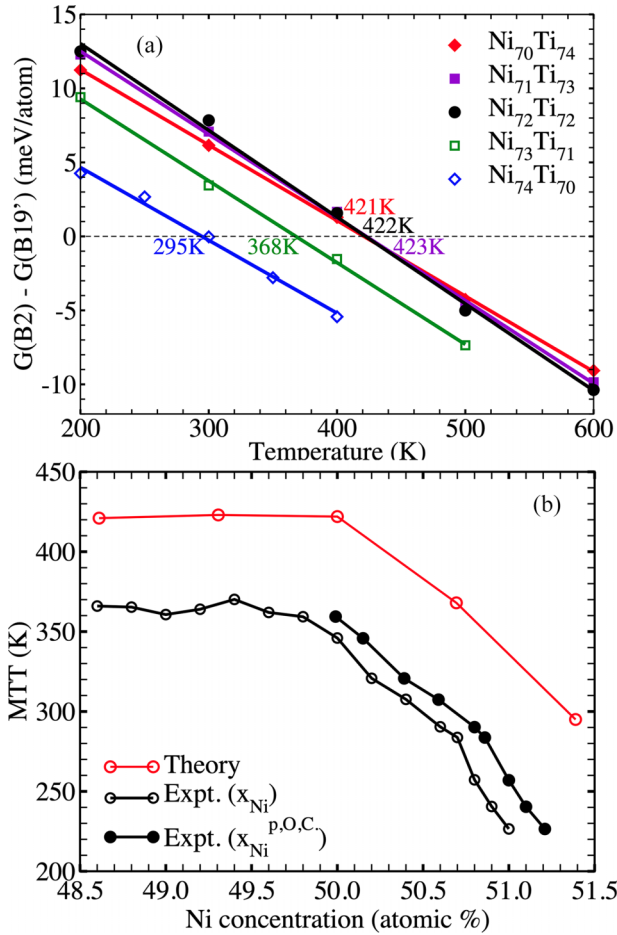


FIG. 4. (a) The Gibbs free energy G difference (ΔG) between the austenite B2 and martensite B19' phases. The martensitic transition temperatures (MTTs) are determined at $\Delta G = 0$ and are plotted in (b) in comparison with experimental data [19]. Note that the open black circles denote the Ni concentration (x_{Ni}) in raw material, while the filled black circles correspond to the purity-corrected Ni concentration ($x_{\text{Ni}}^{\text{p.O.C.}}$).

off-stoichiometric SMAs as in equiatomic binaries, and our current method is equally applicable.

Latent heat. There are two physical quantities to compensate the energy difference (ΔE) between the two phases at the transition temperature. One is the difference in anharmonic energy (E_{anh}) and the other is the entropy (S) difference. One can separate and calculate these two terms following Haskins *et al.* [26,27], i.e., at the transition temperature T ,

$$\Delta E = \Delta E_{\text{anh}} - T\Delta S. \quad (4)$$

Here, ΔE is the electronic energy difference between the reference austenite structure and the corresponding martensite structure, ΔE_{anh} is the anharmonic energy difference, and ΔS is the entropic difference including both vibrational and electronic configurational [S^{el} in Eq. (2)] contributions. We omitted the contribution of ΔU^{el} to ΔE since the magnitude of ΔU^{el} is less than 1 meV/atom for all of these NiTi binaries. E_{anh} is defined as the amount of energy relative to the ideal classical solids, i.e.,

$$E_{\text{anh}}(T) = 1.5k_{\text{B}}T - [\bar{E}(T) + \bar{E}_{\text{kin}}(T) - E_{\text{ref}}(T)], \quad (5)$$

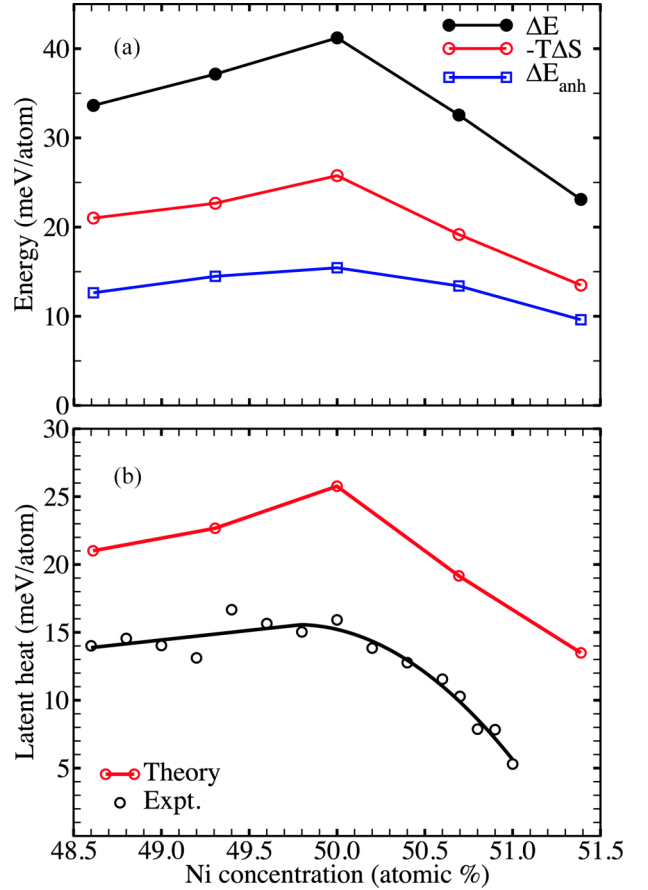


FIG. 5. (a) The calculated energy difference (ΔE), $-T\Delta S$, and the difference in anharmonic energy (E_{anh}) at the transition temperature. (b) The calculated latent heat $q = -T\Delta S$, compared with experimental data [19].

where $\bar{E}(T)$, $\bar{E}_{\text{kin}}(T)$, and $E_{\text{ref}}(T)$ are the mean electronic energy, the mean kinetic energy, and the electronic energy of the reference structure at T . E_{anh} is normally within a few meV/atom for the martensite phase, while it is sizable for the austenite phase. As plotted in Fig. 5(a), ΔE_{anh} comes mainly from E_{anh} of the austenite phase, which helps to compensate ΔE and greatly reduces MTT.

The physical meaning of $-T\Delta S$ at MTT is the latent heat (q). Again, the computed trend of q vs x_{Ni} is in excellent agreement with experiment, as demonstrated in Fig. 5(b), though our first-principles calculations consistently overestimate q by 7–10 meV/atom over the considered range of Ni concentration. We summarized our calculated MTT and q in Table I.

Conclusions. In conclusion, our first-principles calculations not only reproduced the striking asymmetry in martensitic transition temperature in off-stoichiometric NiTi

TABLE I. Calculated martensitic transition temperature (MTT, in K) and the latent heat (q , in meV/atom) vs Ni concentration (x_{Ni} , in atomic %).

x_{Ni}	48.6	49.3	50.0	50.7	51.4
MTT	421	423	422	368	295
q	21.0	22.7	25.8	19.2	13.5

near the 50/50 composition, but it also revealed the physical origin of this mysterious behavior, which is mainly due to the characteristics of the charge distributions in these alloys. In NiTi, Ni atoms have 10 valence electrons and a larger effective atomic size, while Ti atoms have 4 valence electrons and a smaller effective atomic size. Thus, replacing Ti by Ni causes more structural reorganization and a higher level of deviation from the ideal B2 in the austenite reference structure than replacing Ni by Ti. Larger structural reorganization results in a much reduced energy difference between the martensite

and austenite phases, and decreased MTT and latent heat. We conclude that the same trend will be present in other SMAs; an SMA's properties and dynamics will be significantly modified if the concentration of the near stoichiometric metal is above 50%, which has more valence electrons than other metals in the SMA.

Acknowledgment. This work was supported by funding from the NASA Aeronautics Research Mission Directorate's (ARMD) Transformational Tools and Technologies (TTT) project.

-
- [1] K. Otsuka and T. Kakeshita, Science and technology of shape-memory alloys: New developments, *MRS Bull.* **27**, 91 (2002).
- [2] J. Mohd Jani, M. Leary, A. Subic, and M. A. Gibson, A review of shape memory alloy research, applications and opportunities, *Mater. Design (1980-2015)* **56**, 1078 (2014).
- [3] P. S. Lobo, J. Almeida, and L. Guerreiro, Shape memory alloys behaviour: A review, *Proc. Eng.* **114**, 776 (2015).
- [4] J. A. Shaw and S. Kyriakides, Thermomechanical aspects of NiTi, *J. Mech. Phys. Solids* **43**, 1243 (1995).
- [5] T. Duerig, 6.1 - The metallurgy of nitinol as it pertains to medical devices, in *Titanium in Medical and Dental Applications*, Woodhead Publishing Series in Biomaterials, edited by F. H. Froes and M. Qian (Woodhead, Sawston, United Kingdom, 2018), pp. 555–570.
- [6] O. Benafan, M. R. Moholt, M. Bass, J. H. Mabe, D. E. Nicholson, and F. T. Calkins, Recent advancements in rotary shape memory alloy actuators for aeronautics, *Shape Mem. Superelastic.* **5**, 415 (2019).
- [7] J. Ma, I. Karaman, and R. D. Noebe, High temperature shape memory alloys, *Intl. Mater. Rev.* **55**, 257 (2010).
- [8] T. Fukuda, T. Saburi, T. Chihara, and Y. Tsuzuki, Mechanism of B2-B19-B19'; transformation in shape memory Ti-Ni-Cu alloys, *Mater. Trans., JIM* **36**, 1244 (1995).
- [9] T. H. Nam, T. Saburi, Y. Nakata, and K. Shimizu, Shape memory characteristics and lattice deformation in Ti-Ni-Cu alloys, *Mater. Trans., JIM* **31**, 1050 (1990).
- [10] R. Zarnetta, R. Takahashi, M. L. Young, A. Savan, Y. Furuya, S. Thienhaus, B. Maaß, M. Rahim, J. Frenzel, H. Brunken, Y. S. Chu, V. Srivastava, R. D. James, I. Takeuchi, G. Eggeler, and A. Ludwig, Identification of quaternary shape memory alloys with near-zero thermal hysteresis and unprecedented functional stability, *Adv. Funct. Mater.* **20**, 1917 (2010).
- [11] A. N. Bucsek, G. A. Hudish, G. S. Bigelow, R. D. Noebe, and A. P. Stebner, Composition, compatibility, and the functional performances of ternary nitix high-temperature shape memory alloys, *Shape Mem. Superelastic.* **2**, 62 (2016).
- [12] O. Benafan, A. Garg, R. Noebe, G. Bigelow, S. Padula, D. Gaydos, N. Schell, J. Mabe, and R. Vaidyanathan, Mechanical and functional behavior of a Ni-rich Ni_{50.3}Ti_{29.7}Hf₂₀ high temperature shape memory alloy, *Intermetallics* **50**, 94 (2014).
- [13] S. Liu, B. B. Kappes, B. Amin-ahmadi, O. Benafan, X. Zhang, and A. P. Stebner, Physics-informed machine learning for composition - process - property design: Shape memory alloy demonstration, *Appl. Mater. Today* **22**, 100898 (2021).
- [14] W.-C. Kim, K.-R. Lim, W.-T. Kim, E.-S. Park, and D.-H. Kim, Recent advances in multicomponent NiTi-based shape memory alloy using metallic glass as a precursor, *Prog. Mater. Sci.* **123**, 100855 (2022).
- [15] O. Benafan, G. S. Bigelow, A. Garg, L. G. Wilson, R. B. Rogers, E. J. Young-dohe, D. F. Johnson, D. A. Scheiman, J. W. Lawson, and Z. Wu, Ultra high temperature shape memory behavior in Ni-Ti-Hf alloys, unpublished (2023).
- [16] G. R. Purdy and J. G. Parr, A study of the titanium-nickel system between Ti₂Ni and TiNi, *Trans. Met. Soc. AIME* **221**, 636 (1961).
- [17] R. Wasilewski, S. Butler, and J. Hanlon, Homogeneity range and the martensitic transformation in TiNi, *Metall. Trans.* **2**, 229 (1971).
- [18] J. D. Harrison and D. E. Hodgson, Use of TiNi in mechanical and electrical connectors, in *Shape Memory Effects in Alloys*, edited by J. Perkins (Springer, Boston, MA, 1975), pp. 517–523.
- [19] J. Frenzel, E. George, A. Dlouhy, C. Somsen, M.-X. Wagner, and G. Eggeler, Influence of Ni on martensitic phase transformations in NiTi shape memory alloys, *Acta Mater.* **58**, 3444 (2010).
- [20] X. Huang, G. J. Ackland, and K. M. Rabe, Crystal structures and shape-memory behaviour of NiTi, *Nat. Mater.* **2**, 307 (2003).
- [21] C. Gong, Y. Li, Y. Wang, and D. Yang, *Ab initio* study for electronic and crystal structure of NiTi r-phase, *Modell. Simul. Mater. Sci. Eng.* **14**, 33 (2006).
- [22] N. Hatcher, O. Y. Kontsevoi, and A. J. Freeman, Martensitic transformation path of NiTi, *Phys. Rev. B* **79**, 020202(R) (2009).
- [23] N. Hatcher, O. Y. Kontsevoi, and A. J. Freeman, Role of elastic and shear stabilities in the martensitic transformation path of NiTi, *Phys. Rev. B* **80**, 144203 (2009).
- [24] K. Guda Vishnu and A. Strachan, Phase stability and transformations in NiTi from density functional theory calculations, *Acta Mater.* **58**, 745 (2010).
- [25] J. B. Haskins, A. E. Thompson, and J. W. Lawson, *Ab initio* simulations of phase stability and martensitic transitions in NiTi, *Phys. Rev. B* **94**, 214110 (2016).
- [26] J. B. Haskins and J. W. Lawson, Finite temperature properties of NiTi from first principles simulations: Structure, mechanics, and thermodynamics, *J. Appl. Phys.* **121**, 205103 (2017).
- [27] J. B. Haskins, H. Malmir, S. J. Honrao, L. A. Sandoval, and J. W. Lawson, Low-temperature mechanical instabilities govern high-temperature thermodynamics in the austenite phase of shape memory alloy constituents: *Ab initio* simulations of NiTi, NiZr, NiHf, PdTi, and PtTi, *Acta Mater.* **212**, 116872 (2021).

- [28] W.-S. Ko, Temperature dependence of NiTi martensite structures: Density functional theory calculations, *Scr. Mater.* **154**, 134 (2018).
- [29] S. Kadhodaei and A. van de Walle, First-principles calculations of thermal properties of the mechanically unstable phases of the PtTi and NiTi shape memory alloys, *Acta Mater.* **147**, 296 (2018).
- [30] P. Kumar and U. V. Waghmare, First-principles phonon-based model and theory of martensitic phase transformation in NiTi shape memory alloy, *Materialia* **9**, 100602 (2020).
- [31] G. Eggeler, *Material Science and Engineering of NiTi Shape Memory Alloys: Fundamentals, Microstructure, Processing and Applications*, 1st ed. (Wiley-VCH, 2020).
- [32] Z. Wu and J. W. Lawson, Theoretical investigation of phase transitions in the shape memory alloy NiTi, *Phys. Rev. B* **106**, L140102 (2022).
- [33] X. Zhang, B. Grabowski, F. Körmann, C. Freysoldt, and J. Neugebauer, Accurate electronic free energies of the 3d, 4d, and 5d transition metals at high temperatures, *Phys. Rev. B* **95**, 165126 (2017).
- [34] G. Kresse and J. Hafner, *Ab initio* molecular dynamics for liquid metals, *Phys. Rev. B* **47**, 558 (1993).
- [35] G. Kresse and J. Hafner, *Ab initio* molecular-dynamics simulation of the liquid-metal–amorphous–semiconductor transition in germanium, *Phys. Rev. B* **49**, 14251 (1994).
- [36] G. Kresse and J. Furthmüller, Efficiency of *ab initio* total energy calculations for metals and semiconductors using a plane-wave basis set, *Comput. Mater. Sci.* **6**, 15 (1996).
- [37] G. Kresse and J. Furthmüller, Efficient iterative schemes for *ab initio* total-energy calculations using a plane-wave basis set, *Phys. Rev. B* **54**, 11169 (1996).
- [38] B. Grabowski, L. Ismer, T. Hickel, and J. Neugebauer, *Ab initio* up to the melting point: Anharmonicity and vacancies in aluminum, *Phys. Rev. B* **79**, 134106 (2009).
- [39] J. P. Perdew, K. Burke, and M. Ernzerhof, Generalized gradient approximation made simple, *Phys. Rev. Lett.* **77**, 3865 (1996).
- [40] P. E. Blöchl, Projector augmented-wave method, *Phys. Rev. B* **50**, 17953 (1994).
- [41] G. Kresse and D. Joubert, From ultrasoft pseudopotentials to the projector augmented-wave method, *Phys. Rev. B* **59**, 1758 (1999).
- [42] G. M. Michal and R. Sinclair, The structure of TiNi martensite, *Acta Crystallogr. Sect. B* **37**, 1803 (1981).
- [43] W. Buhner, R. Gotthardt, A. Kulik, O. Mercier, and F. Staub, Powder neutron diffraction study of nickel-titanium martensite, *J. Phys. F: Met. Phys.* **13**, L77 (1983).
- [44] R. R. Pezarini, H. S. Bernabé, F. Sato, L. C. Malacarne, N. G. C. Astrath, J. H. Rohling, A. N. Medina, R. D. dos Reis, and F. C. G. Gandra, On the use of photothermal techniques to study NiTi phase transitions, *Mater. Res. Express* **1**, 026502 (2014).
- [45] V. Shastry, V. Divya, M. Azeem, A. Paul, D. Dye, and U. Ramamurty, Combining indentation and diffusion couple techniques for combinatorial discovery of high temperature shape memory alloys, *Acta Mater.* **61**, 5735 (2013).
- [46] W. Cai and K. Otsuka, Martensite aging effect and thermal cyclic characteristics in Ti-Pd and Ti-Pd-Ni high temperature shape memory alloys, *J. Mater. Sci. Technol.* **17**, 359 (2001).
- [47] Z. Wu, H. Malmir, O. Benafan, and J. W. Lawson, Predicting the martensitic transition temperatures in ternary shape memory alloys $\text{Ni}_{0.5}\text{Ti}_{0.5-x}\text{HF}_x$ from first principles, *Acta Mater.* **261**, 119362 (2023).
- [48] O. Hellman, I. A. Abrikosov, and S. I. Simak, Lattice dynamics of anharmonic solids from first principles, *Phys. Rev. B* **84**, 180301(R) (2011).
- [49] O. Hellman, P. Steneteg, I. A. Abrikosov, and S. I. Simak, Temperature dependent effective potential method for accurate free energy calculations of solids, *Phys. Rev. B* **87**, 104111 (2013).